

A mechanism to explain the generation of earthquake lights

D. A. Lockner, M. J. S. Johnston & J. D. Byerlee

US Geological Survey, 345 Middlefield Road, Menlo Park, California 94025, USA

Explanations of how earthquake lights might arise have failed to show how large charge densities can be concentrated and sustained in a conductive Earth. A physical model is proposed, based on frictional heating of the fault, that solves this and related problems.

EARTHQUAKE LIGHTS (EQLs) have long been an unexplained problem in seismology. Early on, the very existence of EQL was questioned by the scientific community since no really 'testable' data existed and observations were invariably made by untrained observers. A transformation in these attitudes occurred when photographs of luminous phenomena were taken during the Matsushiro earthquake swarm in Japan (Fig. 1), between 1965 and 1967^{1,2}. The reluctance to accept the proposal that large-scale electromagnetic disturbances are associated with earthquakes has been supported by the lack of any satisfactory theory to explain how large charge concentrations can be generated and maintained in a highly conductive Earth. However, the continuing reports of EQL³⁻⁷, especially the Matsushiro pictures, have led to a general acknowledgement that EQLs do occur. Numerous mechanisms for generating EQL have been investigated. Because many crustal rocks are quartz rich, piezoelectric effects have received much attention⁸, although this mechanism has generally been discounted because of both the short decay time constant of the piezoelectric process⁹ and indications that piezoelectric charges may be self-cancelling¹⁰. Mizutani *et al.*¹¹ have discussed the possible role of streaming potentials produced by movement of groundwater. However, the problem remains of demonstrating a mechanism that provides for the concentration and maintenance of large charge densities near the Earth's surface. The charge relaxation time for electrostatic processes is ϵ/σ where σ is conductivity and ϵ is permittivity (typically, $\epsilon = 0.5-1.0 \times 10^{-10} \text{ F m}^{-1}$ for crustal rocks)¹². For a relaxation time of 1 s, a conductivity below $10^{-10} \text{ S m}^{-1}$ is required and is not normally found in the Earth's crust. The following theory is proposed as a solution to this dilemma.

Note that EQL phenomena do not accompany all earthquakes, indeed it seems to be the exception rather than the rule. A significant observation has been made by seismologists in the People's Republic of China. In a recent compilation of world-wide reports of EQL¹³, most occurrences were for earthquakes of magnitude 7 or greater, with only a few in the range $M = 6$ to 7 and none below $M = 5$. This provides an important test constraint for our theory.

Friction-vaporization theory

We suggest that during a large earthquake significant frictional heating of the shear zone will occur. In the proper conditions, this will lead to vaporization of water in and near the shear zone and a dramatic decrease in electrical conductivity, σ , for saturated or partially saturated rock from about 10^{-1} to $<10^{-10} \text{ S m}^{-1}$. Together with lowered conductivity, the intense shearing and the vaporization of porewater produces significant charge separation in the shear zone. Continued frictional heating produces increasing σ in the shear zone (10^{-5} S m^{-1} at 500°C ; 10^{-4} S m^{-1} at 650°C) resulting in a central conductor

central conductor will collect charge in the shear zone, and because it is hundreds of metres deep and only centimetres wide, it will concentrate the charge along its edges, where the curvature is highest. If the conductor is shallow enough, the charge concentrated along its top edge will produce an intense electric field at the Earth's surface, enhanced by the normal atmospheric potential gradient, that will then be strong enough to induce coronal discharge in the atmosphere above the fault.

Heating of fault

Various aspects of frictional heating of faults during earthquakes have recently received much attention¹⁴⁻¹⁸. Although the efficiency of frictional heating during earthquakes and the vertical distribution of stress on active faults are topics of much controversy, Sibson *et al.*¹⁹ have shown through identification of pseudotachylytes that significant frictional melting does occur on some faults. Measurements on laboratory samples²⁰ show that >90% of the energy released in stick-slip is used in frictional heating of the fault. So we can assume that, at least for some earthquakes, significant heating of the fault zone will occur.

Conductivity of rock

The study of the electrical properties of rock in a variety of geological conditions is still in its early stages, but many useful data already exist. Olhoeft^{21,22} has measured resistivity (equal to σ^{-1}) as a function of temperature for granite, basalt and hornblende schist. At 100°C , σ for vacuum dry granite is $10^{-12} \text{ S m}^{-1}$, that is >10 orders of magnitude lower than wet granite. (Similar results were found for the other rock types.) Although it may seem unexpected, as water-saturated granite is heated above 100°C at 1 atm, conductivity will approach $10^{-12} \text{ S m}^{-1}$ even though water vapour is still present in the pores.

Water vapour is often thought to be a good electrical conductor. For example, it is well known that in humid weather, conductivity of insulators will significantly increase. However, this apparent increase in conductivity is due to surface conduction in water adsorbed onto the surface of the insulator and not to volume conduction in the vapour phase. If the adsorbed water is removed through heating or evacuation, surface conduction will be significantly reduced. Steam and water vapour are in fact very good insulators with $\sigma < 10^{-14} \text{ S m}^{-1}$ (ref. 23). Rust and Moore²⁴ have measured electrical relaxation times more than 6 times greater at the base of thunderclouds than in clear air, indicating that clouds have a conductivity of the order of $10^{-15} \text{ S m}^{-1}$ (ref. 25). In fact, this is why clouds can sustain very large charge separation. Thus, for most partially saturated rocks, surface conduction has the primary role in determining conductivity.

of vacuum dry rock even when some adsorbed water remains. The first monolayers of water (including the outer Helmholtz plane, OHP) are tightly bound to crystal surfaces²⁶, so that even though some surface conduction occurs in this region, it is much less than the conduction that occurs in the more mobile layers beyond the OHP. Thus, for wet granite with pore pressure below the critical pressure of 22 MPa and at temperatures sufficient to vaporize the water, conductivity will be within one order of magnitude of the vacuum dry conductivity²³. Data for granite²² are reproduced in Fig. 2 together with a curve of estimated conductivity at 1 atmosphere pore pressure.

Charge source

Numerous mechanisms have been suggested as potential sources of charge for EQLs. Piezoelectricity and streaming potential have already been mentioned here. Due to the intense shearing inherent in earthquakes, triboelectric processes must also occur²⁷. However, the primary source of charge in our model is the vaporization of porewater during the intense shearing and heating of the fault zone. It has long been known that mechanical disruption of water droplets can produce large charges^{28,29}. The charging of water droplets by splashing or spraying was termed 'waterfall electrification' by Lenard³⁰ or by others, 'Lenard splashing'. It has also been referred to as 'balloelectrification'³¹ and 'spray electrification'³². These terms all refer to the disruption of liquid surfaces and can generate hundreds or thousands of volts. For example, explosions on supertankers at sea have occurred while being washed down with a high-power waterjet. Pierce³³ suggested the electrical charging that was developed through Lenard splashing during the washing operations was probably the cause of the discharge that ignited oil vapour and resulted in these disasters. Although this manner of separating charge is a well documented experimental phenomenon, the mechanism by which the charge is produced is not well understood. It is thought to be related to the sudden disruption of the surface layer in non-equilibrium conditions. When a new surface is created a liquid will spontaneously form a structured boundary layer whose chemical and electrical gradients differ from those of the interior of the fluid. The equilibrium distribution of ions, as well as the rate at which the boundary layer forms, will depend on the types and concentration of ions in solution. If a segment of the boundary layer is suddenly removed (by violent boiling, for example) the net charge of the resulting droplet can be very different from that of the host. Blanchard³⁴ has, in fact, found that the mechanical tearing apart of water during violent boiling

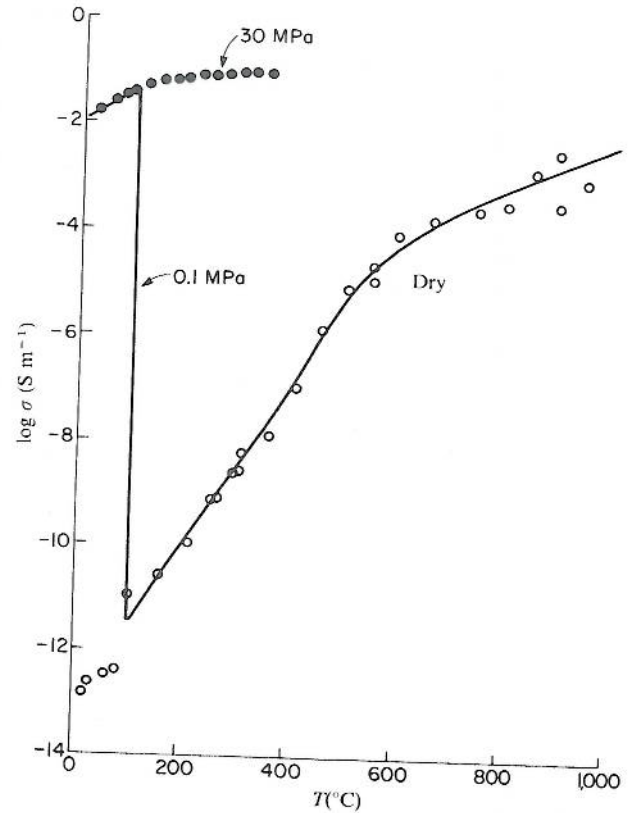


Fig. 2 Log conductivity against temperature for granite at 0.1 MPa pore pressure (data taken from ref. 22). The abrupt drop in σ at the boiling point should occur for pressures below the critical pressure (22 MPa). Open symbols are vacuum dry; closed symbols are water-saturated rock at 30 MPa.

generates charges up to 10^{-7} C g⁻¹ of evaporated water. As an example below will show, this process can provide a charge sufficient for the requirements of our model.

In applying our theory, many plausible geometries can be used that would produce circumstances favourable for EQL or other electromagnetic phenomena. For a vertical fault plane in which $\frac{\partial T}{\partial z} \ll \frac{\partial T}{\partial x}$ (where x is perpendicular to the fault and z increases with depth), temperature $T(x, t)$ satisfies¹⁷

$$\frac{\partial T}{\partial t} = \frac{A}{\rho c} + \alpha \frac{\partial^2 T}{\partial x^2} \quad (1)$$

where A is the heat source, ρc the volumetric specific heat and α the thermal diffusivity. The temperature $T(0, t)$ on the axis of a uniformly sheared fault during slip is given by¹⁷

$$T(0, t) = \frac{\tau v}{2\rho c a} \left[1 - 4i^2 \operatorname{erfc} \frac{a}{a_T} \right] \quad (2)$$

where

$$i^n \operatorname{erfc} x = \int_x^\infty i^{n-1} \operatorname{erfc} \epsilon \, d\epsilon \quad (2a)$$

$$i^0 \operatorname{erfc} x = \operatorname{erfc} x = 1 - \operatorname{erf} x \quad (2b)$$

and where τ = shear stress, v = average sliding velocity, a = fault half width and $a_T(t) = \sqrt{4\alpha t}$ is the conduction half width. Following the earthquake (duration time = t^*), we calculate temperatures in one of two ways. For $a/a_T^* < 1$, the source is diffusion dominated and we approximate it by an instantaneous release of heat per unit area = $\tau v t^*$ at $x = 0$, $t = t^*/2$. The temperature distribution is given by³⁵

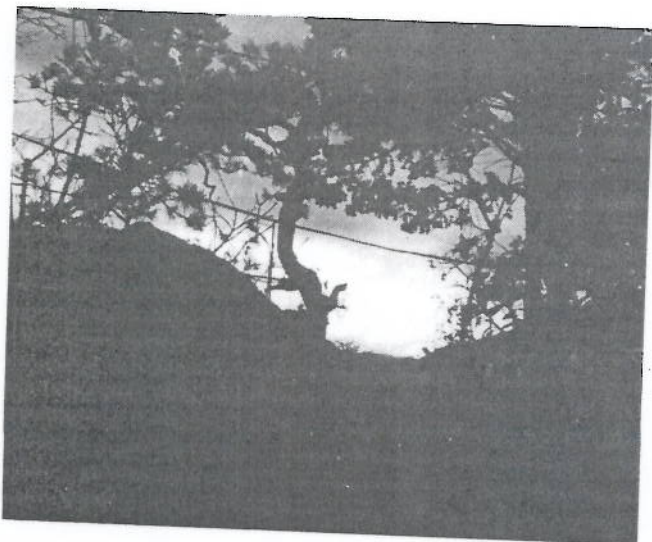


Fig. 1 Photograph taken 16 s after beginning of EOI at Mat.

where $t' = t - t^*/2$ and $a'_\pm = \sqrt{4\alpha t'}$. For $a/a^*_\pm > 1$, conduction of heat out of the shear zone is not important during the earthquake. In this case, the source is approximated by a region of width $2a$ and of uniform temperature at time $t^*/2$. The solution is given by

$$T(x, t') = \frac{\tau v t^*}{4\rho c a} \left[\operatorname{erf} \frac{a-x}{a'_+} + \operatorname{erf} \frac{a+x}{a'_-} \right] \quad (4)$$

The approximations (3) and (4) give errors $< 10\%$ for $t = 2t^*$ and rapidly converge on the correct solution for $t > 2t^*$. Equation (2) gives the axial temperature for $t \leq t^*$ exactly.

Values of the parameters used in the example are

$$\alpha = 0.01 \text{ cm}^2 \text{ s}^{-1} \quad (5a)$$

$$\rho c = 0.65 \text{ cal cm}^{-3} \text{ }^\circ\text{C}^{-1} \quad (5b)$$

$$v = 200 \text{ cm s}^{-1} \quad (5c)$$

$$\mu = 0.48 \quad (5d)$$

$$T_g = 10 + 30z \text{ }^\circ\text{C km}^{-1} \quad (5e)$$

Equations (5a), (5b), and (5d) are typical values found for crustal rocks¹⁷. The coefficient of friction μ is within the range of values measured both in the field and in the laboratory for San Andreas Fault gouge. Laboratory measurements indicate that in regions lacking clay-rich gouge, μ can be as large as 0.80. This would make near-surface frictional heating even more intense than we assume in the present model. Equation (5c) is generally assumed to represent an earthquake stress drop of 20 MPa (ref. 36). Although earthquake stress drops commonly range from 1 to 10 MPa (representing velocities between 10 and 100 cm s^{-1} , 20 MPa is a plausible value. In fact, one implication of our model is that during moderate earthquakes, EQL would be more likely to occur when stress drops are above average.

A thermal gradient of $30 \text{ }^\circ\text{C km}^{-1}$ (equation (5e)) is added to all temperatures, although this has little effect on the near-surface phenomena. Also, we assume a 100 m unsaturated zone above the water table. The main effect of having such a low water table is to increase the near-surface effective pressure (= normal stress - pore pressure), and consequently increase the shear stress. By using a 100-m water table, shear stress at 100 m depth is 20% higher than if the water table were at the surface. Because other parameters can affect the near-surface heating, the precise depth of the water table is not critical. Effects due to heat of vaporization as water is flashed to steam are ignored here. For a shear zone containing 1% water, neglecting heat of vaporization results in at most an $8 \text{ }^\circ\text{C}$ error and for the purposes of the present example is unimportant. If water content were 10%, errors of as much as $80 \text{ }^\circ\text{C}$ could result and other processes (such as transport of heat by migration of water from the fault zone) may become important. To avoid these complications, we assume a porosity of only a few per cent. Complex effects resulting from ejection of steam from the fault zone are ignored. We further assume that pore pressure in the region of interest remains below 22 MPa because of undersaturation, dilatancy of the fault zone, high permeability¹⁷, or hydrofracture³⁷.

To estimate the stress distribution, the best data to draw on are probably those of McGarr *et al.*³⁸, who determined that static shear stress (τ_s) in the top 1 km of the crust parallel to the San Andreas Fault is

$$\tau_s = (0.90 \pm 0.47)(\text{MPa}) + (7.86 \pm 1.18)(\text{MPa km}^{-1})z \quad (6)$$

The dynamic shear stress τ measured along the fault during sliding should in general be $< \tau_s$. However, depending on the composition of the fault gouge material, the coefficient of friction can be much greater than equation (5d). As a result, dynamic shear stress in other regions could be greater than would be calculated by equation (6). The amount of energy going into frictional heating

heating to be $> 90\%$ efficient for low normal stress events. Thus, for the sake of simplicity, using equations (5d) and (6) and a 100-m unsaturated zone, we take

$$\tau = 1.0(\text{MPa}) + 13.0(\text{MPa km}^{-1})z \quad z \leq 0.1 \text{ km} \quad (7a)$$

$$\tau = 1.5(\text{MPa}) + 8.0(\text{MPa km}^{-1})z \quad z > 0.1 \text{ km} \quad (7b)$$

In (equation (7a)), pore pressure above the water table is 0 and both effective pressure and shear stress increase faster than below the water table (equation (7b)) where pore pressure increases with depth.

The processes controlling fault width are poorly understood, so our choice of the width of the shear zone, $2a$, must be somewhat arbitrary. In a study of fault zone characteristics for faults as deep as 5 km in North America, Wallace and Morris³⁹ make several generalizations. They find that the widths of fault zones tend to be greater for faults having greater displacements. Faults are generally constituted of one or more claylike gouge zones in a matrix of sheared and foliated rock that is bordered by highly fractured rock. They also find the width of the gouge zone generally to be 1/100 to 1/300 the total displacement and the width of the highly fractured zone to be ~ 10 times that of the gouge zone. From similar observations Robertson⁴⁰ has found a strong correlation between total slip, u , and fault width. He finds that $2a/u$ averages 1/100 and can range in value from 1/10 to 1/1,000. He also observes that many of the fault zones with low $2a/u$ were shallow and (presumably) at low stress. Furthermore, studies of wear in metals (little work of this nature has been done with rocks) indicate that the rate of production of wear particles is proportional to stress⁴¹. We assume, in the absence of better data, that for a single earthquake the shear zone width on a fault will be proportional to displacement and stress. Relating shear stress to depth, we use in our example

$$2a(\text{cm}) = 2 \times 10^{-2} u(\text{cm})z(\text{km}) \quad (8)$$

For earthquakes of $M = 6, 7$ and 8 , we use slip $u = 29, 130$, and 620 cm , respectively. $\sigma(T)$ is taken from Fig. 2 (using the data of Olhoeft²²). Some key parameters in the example are listed in Table 1.

Figure 3a-d plots conductivity contours for different stages of an $M = 8$ earthquake. These were obtained by first calculating temperature from equations (2), (3) and (4) and then converting to conductivity by means of Fig. 2. The wedge shape contours in Fig. 3a, plotted at the end of the earthquake ($t^* = 3.1 \text{ s}$), outline the shear zone, which in this example increases linearly with depth. Outside the shear zone, $\sigma > 10^{-2} \text{ S m}^{-1}$. On the edges of the shear zone, temperature rises

Table 1 Model parameters

	z (km)	τ (MPa)	a (cm)	$T(0, t^*)$ ($^\circ\text{C}$)	$\sigma(0, t^*)$ (S m^{-1})
$M = 8$	0.001	10.1	0.01	738	4×10^{-4}
$u = 620 \text{ cm}$	0.01	11.3	0.06	715	3×10^{-4}
$v = 200 \text{ cm s}^{-1}$	0.02	12.6	0.12	681	2×10^{-4}
$t^* = 3.1 \text{ s}$	0.05	16.5	0.31	566	3×10^{-5}
	0.1	23.0	0.62	435	4×10^{-7}
	0.5	55.0	3.10	227	3×10^{-10}
$M = 7$	0.001	10.1	0.00	346	1×10^{-8}
$u = 130 \text{ cm}$	0.01	11.3	0.01	362	2×10^{-8}
$v = 200 \text{ cm s}^{-1}$	0.02	12.6	0.03	375	4×10^{-8}
$t^* = 0.65 \text{ s}$	0.05	16.5	0.06	396	8×10^{-8}
	0.1	23.0	0.13	389	7×10^{-8}
	0.5	55.0	0.65	227	3×10^{-10}
$M = 6$	0.001	10.1	0.00	170	4×10^{-11}
$u = 29 \text{ cm}$	0.01	11.3	0.00	183	6×10^{-11}
$v = 200 \text{ cm s}^{-1}$	0.02	12.6	0.01	197	9×10^{-11}
$t^* = 0.145 \text{ s}$	0.05	16.5	0.01	231	3×10^{-10}

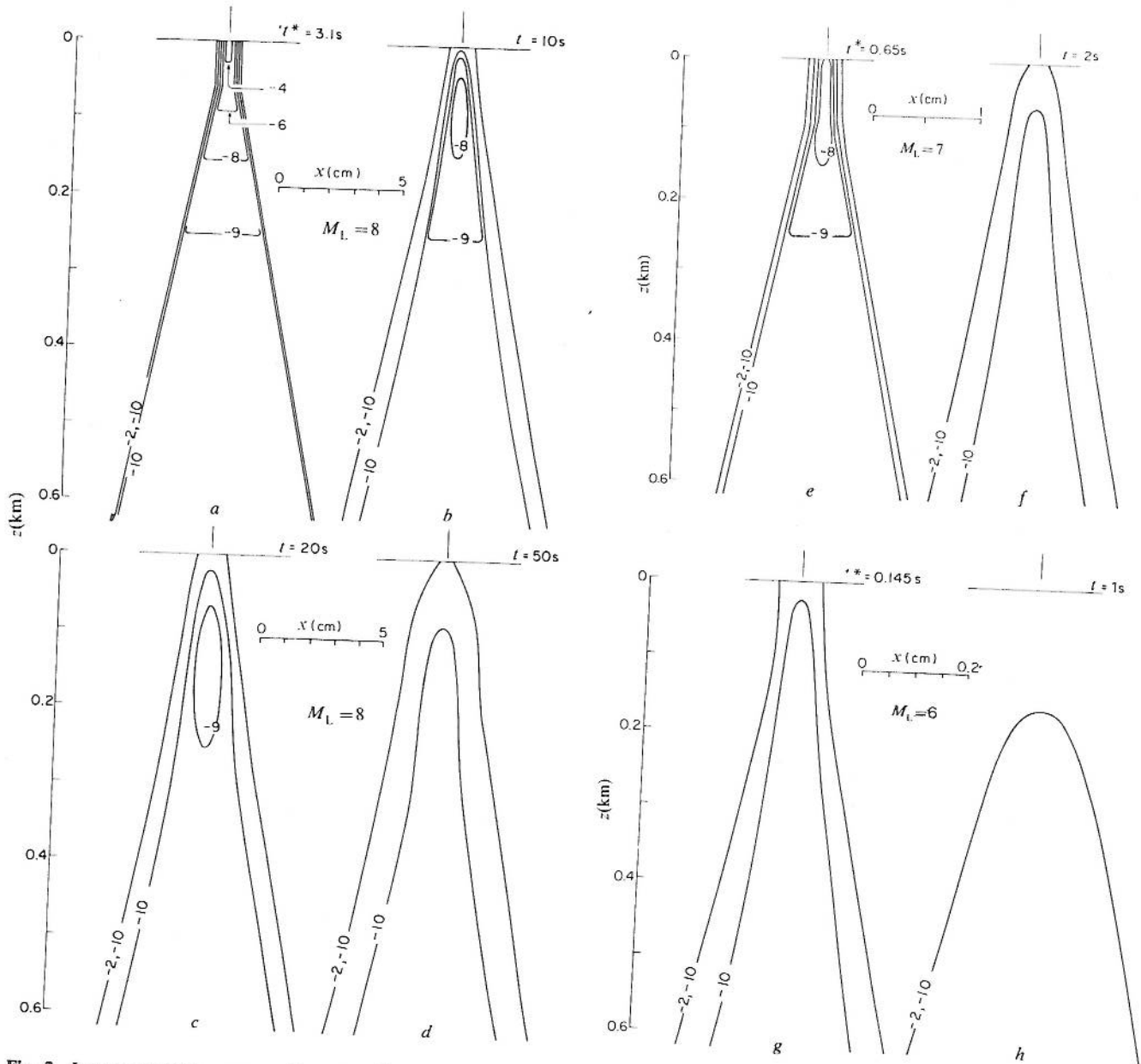


Fig. 3 Log-conductivity cross-sections (S m^{-1}) for various earthquakes $v = 200 \text{ cm s}^{-1}$, a-d, $M = 8$; horizontal exaggeration = 15,400:1. e, f, $M = 7$, horizontal exaggeration = 15,400:1. g, h, $M = 6$ horizontal exaggeration = 69,000:1; shear zone has not heated enough to form central conductor.

abruptly ($a^* = 0.4 \text{ cm}$) and $\sigma < 10^{-11}$ as water is vaporized. In the interior, temperature approaches 740°C and conductivity increases to $4 \times 10^{-4} \text{ S m}^{-1}$ near the surface, where slip is accommodated by the narrowest shear zone. The central conductor actually reaches the surface, extends to a depth of 100–200 m and averages $\sim 1 \text{ cm}$ in width. Such a narrow near-surface shear zone is not uncommon¹⁶. Below 400 m, temperature in the shear zone changes little with depth because increasing stress is balanced by increasing fault width. This leaves the conducting region bounded by an insulator $\sigma < 10^{-11} \text{ S m}^{-1}$ on the sides and $\sigma < 10^{-9.5} \text{ S m}^{-1}$ underneath. The low conductivity region in the shear zone below 400 m depends on the ratio of stress to fault width and could be decreased by 2 orders of magnitude by choosing a more complex depth dependence for these parameters. Conductivity will also vary with mineralogy. For example, conductivity of $10^{-12} \text{ S m}^{-1}$ was reported for magnetite-free dunite⁴² at 200°C . Also, increasing quartz content will tend to decrease conductivity. Thus, σ can easily vary by 2 orders of magnitude above or below the curve drawn in Fig. 2. As water vaporizes, the shear zone becomes

left oppositely charged. After 10 s (Fig. 3b), the central conductor has disappeared as the near-surface shear zone cools. However, any charge accumulated in this region will be trapped in what now has become a low conductivity zone until the water vapour can recondense. Figure 3d plots conductivity at 50 s, just before water vapour in the surface layer recondenses and shields any remaining charge from the atmosphere.

To estimate the charge that would accumulate near the surface, let us assume that porosity is 1% and that the vaporized water in the central conductor (Fig. 3a) provides 10^{-7} C g^{-1} of charge³⁴. Note that although the central conductor in Fig. 3a appears wedge-shaped, horizontal exaggeration is 3,230:1 and the true width-to-depth ratio is about 10^{-4} . Thus most of the charge will concentrate along the high-curvature edges of the conductor and will be further concentrated near the surface by the natural geopotential gradient. If all of this charge were concentrated in a 1-cm wide surface zone, the charge density would be $2 \times 10^{-11} \text{ C m}^{-2}$, much greater than the $5 \times 10^{-5} \text{ C m}^{-2}$ required to cause coronal discharge in air above a potential of 7

irregularities would further concentrate the charge, and so would enhance this effect.

Figure 3e, f plots conductivity for a $M = 7$ earthquake. As in the previous example, the insulating layer reaches the surface. However, because of the decrease in total slip, the near-surface zone does not get as hot as it did in the $M = 8$ example. Consequently, the central conductor only begins to form and surface charge concentration will be much less than in the previous example. Also, the charge concentration will be shielded from the atmosphere after only 2 s (Fig. 3f). Figure 3g, h plots conductivity for a $M = 6$ earthquake. In this example, no central conductor develops, and so any mechanism for concentrating charge from large sections of the fault is eliminated. Our model shows that a $M = 7$ earthquake is the smallest that we would expect to produce EQL in the conditions presented in these examples. This agrees with the observations, stated earlier, that EQL primarily occur during earthquakes of $M \geq 7$.

Conclusions

We have shown that with quite reasonable physical assumptions, EQL can be generated and should be expected for at least some earthquakes. Since our mechanism for producing EQL is a near-surface phenomenon even for very large earthquakes, we would not expect these effects to occur in deep subduction zone earthquakes. This is consistent with the reported observations. Furthermore, since this mechanism is a consequence of substantial energy release during the failure process, EQL are not expected to precede the main shock. In some cases, EQL have been reported to occur moments before the main shock. These observations might be explained in the following manner. A person standing, for example, 60 km from the hypocentre of a large earthquake would first observe either EQL in the distance or perhaps the reflection of EQL off of overlying clouds. However, given a crustal shear wave velocity of $\sim 3 \text{ km s}^{-1}$, he would not feel the earthquake until 20 s later, thereby concluding incorrectly that the lights preceded the earthquake.

It is clear from the examples shown that for EQL to be generated, sufficient heat must be available to vaporize water and to form a central conductor and the pore pressure must remain low. At 10 MPa, for example, the boiling point of water is raised to 311°C , at which point $\sigma = 0.6 \times 10^{-8} \text{ S m}^{-1}$ (Fig. 2). The electrical conductivity will exceed this value at all other temperatures and an insulating sheath will not be formed. Low pore pressure at depth will occur only if the rock has no pore water or if appreciable dilatancy accompanies the earthquake. Measurements of faults³⁹ reveal that gouge zones are generally surrounded by regions of highly fractured rock ~ 10 times wider than the gouge zone. Because this fractured zone increases with increasing fault displacement, it is probably produced during the slip episodes. Consequently, co-seismic dilatancy, low pore pressure, and therefore electromagnetic phenomena may occur hundreds of metres below the surface. Development of the central conductor is strongly dependent on the near-surface shear zone width, stress displacement, and sliding velocity (equation (2)). In the example in Fig. 3a-d, the central conductor would still form for $v = 10 \text{ cm s}^{-1}$. However, for an $M = 7$

earthquake, the shear zone would no longer heat up enough to form a continuous conductor. Although there is sufficient slip in a $M = 8$ earthquake to make EQL possible over a wide range of slip velocities, the smaller slip associated with $M = 6$ to 7 earthquakes reduces the likelihood of EQL unless near-surface heating is enhanced. Large stress-drop earthquakes would have higher slip velocities and would therefore be more likely to generate EQL. Earthquakes resulting from the creation of new faults would generally fall in this class. In fact, the 1975 Haicheng⁶ earthquake, for which lights were reported, ruptured at right angles to the trend of mapped faults in the region suggesting that it may have formed a new fault. Near-surface shear stress can be increased in several ways. Gouge zones that are deficient in clay may have coefficients of friction of 0.8 or more. In such regions, shear strength could increase rapidly with depth. Regions with surface shear stress exceeding 1 MPa (ref. 38) will also have greatly enhanced near-surface heating.

EQL would not be expected to occur with all large shallow earthquakes. However, for all large shallow earthquakes we would expect transient changes in both pressure and electrical conductivity in the region around the fault zone. Secondary effects associated with this process might include rapid changes in groundwater levels and the emission of water vapour and other charged gases (CO_2 , H_2 , He, and so on) from the region around the fault zone. Increases in near-surface humidity and ground fog at the time of the Haicheng earthquake^{6,43} and indications of lights over the ocean⁴⁴ may be related to this. Interestingly, large electric fields would also occur with both the emission of water vapour¹⁵ and of gas²⁹ from the fault zone area. These fields could also result in ground glow⁴⁶ as gases are forced up through the permeable zones around, and perhaps in, the fault zone.

Sources of rapid crustal heating other than fault failure should also result in aspects of the electrical process that has been described here. Possible examples are dyke injection and magma intrusion. While the physical details are less clear, the main feature of the model presented here (the formation of an insulating sheath around the injected dyke) together with the secondary features (water-level changes, gas emission, and so on) resulting from the pressure pulse, should both occur. Dyke injection and magma intrusion may have occurred during the Matushiro earthquake swarm⁴⁷. Because the EQL at the Matushiro swarm are the only known ones not associated with large scale surface rupture or large magnitude earthquakes, these EQL are not easily explained by the fault heating process. An explanation in terms of dyke injection in this old volcanic zone would seem preferable in this case. On the other hand, both the 1975 Haicheng⁶ and the 1975 Hawaii earthquakes⁷ may be good examples of failure-generated EQL. The lights in the latter case were apparently viewed parallel to strike along the coast in a south-west direction.

We conclude that, even if EQL do not occur during a given earthquake, short-term transient electric and magnetic disturbances would result from both the generation and movement of charge and the short-term modification of the conductivity structure around the fault zone. These may provide useful tests of our theory.

Received 28 June 1982; accepted 4 January 1983.

1. Yasui, Y. *Proc. Kakioka Magnetic Observ.* **13**, 23-33 (1968).
2. Yasui, Y. *Proc. Kakioka Magnetic Observ.* **14**, 67-78 (1971).
3. Kondo, G. *Proc. Kakioka Magnetic Observ.* **13**, 11-23 (1968).
4. Yasui, Y. *Proc. Kakioka Magnetic Observ.* **15**, 81-86 (1972).
5. Derr, J. *Bull. seis. Soc. Am.* **63**, 2177-2187 (1973).
6. Raleigh, C. B. *et al. EOS* **58**, 236-272 (1976).
7. Tilling, R. I. *et al. U.S. Geol. Surv. Circ.* **740**, 33 (1976).
8. Finkelstein, D. & Powell, J. *Nature* **228**, 759-760 (1970).
9. Finkelstein, D. *et al. J. geophys. Res.* **78**, 992-993 (1973).
10. Tuck, G. J. *et al. Tectonophysics* **39**, 17-111 (1977).
11. Mizutani, H. *et al. Geophys. Res. Lett.* **3**, 365-368 (1976).
12. Olhoeft, G. R. *U.S. Geol. Surv. Open-File Rep.* 79-993 (1979).
13. Huang, L. & Hanzhen, D. *Earthquake Light 1-140* (Earthquake Press Beijing, China, 1979).
14. McKenzie, D. P. & Brune, J. N. *Geophys. J. R. astr. Soc.* **29**, 75-78 (1972).
15. Raleigh, C. B. in *Proc. Conf. II Experimental Studies of Rock Friction with Application to Earthquake* (eds ...)
16. Lachenbruch, A. H. & Sass, J. H. *J. geophys. Res.* **85**, 6185-6222 (1980).
17. Sibson, R. H. *et al. in The Origin of the Southern Alps* Vol. 18 (eds Walcott, R. I. & Cresswell, M. M.) 55-65 (The Royal Society of New Zealand, 1979).
18. Lockner, D. & Okubo, P. *J. geophys. Res.* (in the press).
19. Olhoeft, G. R. in *Physical Properties of Rocks and Minerals* Ch. 9 (eds Touloukian, Y. S., Judd, W. R. & Roy, R. F.) (McGraw-Hill, New York, 1980).
20. Olhoeft, G. R. *J. geophys. Res.* **86**, 931-936 (1981).
21. Olhoeft, G. R. *Electrical Properties of Rocks and Minerals* (1981).
22. Rust, W. D. & Moore, C. B. *Q. Jl R. met. Soc.* **100**, 450-468 (1974).
23. Moore, C. B. & Vonnegut, B. in *Lightning* Vol 1 (ed. Golde, R. H.) 51-98 (Academic, New York, 1977).
24. Bockris, J. O'M & Reddy, A. K. N. *Modern Electrochemistry* Vol. 2 (Plenum, New York, 1977).
25. Lowell, F. & Rose-Innes, A. C. *Adv. Phys.* **29**, 947-1023 (1980).
26. Chalmers, J. A. *Atmospheric Electricity* 515 (Pergamon, Oxford, 1976).
27. Matteson, M. J. *J. Colloid and Interface Science* **37**, 879-890 (1971).

33. Pierce, E. T. *Stanford Res. Inst. Rep. 4454* to O.N.R. Contract No. 0014-71-C-0106 (December 1970).
34. Blanchard, D. C. *Nature* **201**, 1164-1166 (1964).
35. Carslaw, H. S. & Jaeger, J. C. *Conduction of Heat in Solids*, 386 (Oxford University Press, New York, 1959).
36. Brune, J. N., *J. geophys. Res.* **75**, 4997-5009 (1970).
37. Sibson, R. H. *Maurice Ewing Ser. 4 Am. geophys. Un.* 593-603 (1981).
38. McGarr, A., et al. *J. geophys. Res.* **87**, 7797-7806 (1982).
39. Wallace, R. E. & Morris, H. T. in *Proc. Conf. VIII, Analysis of Actual Fault Zones in Bedrock*, (U.S. Geological Survey Open-File Rep. 79-1239, 79-100 1979).
40. Robertson, E. C. *Min. Engng* (in the press).
41. Rabinowicz, E. *Friction and Wear of Materials* (Wiley, New York, 1965).
42. Parkhomenko, E. I. *Rev. Geophys. Space Phys.* **20**, 193-218 (1982).
43. Gu, J. *A Physical Explanation of Imminent Precursory Phenomena: Stable Fault Propagation and Pore Fluids Rise Model* (Preprint, Harvard University, 1981).
44. Wallace, R. E. et al. *Geol. Soc. Am. Abstr. Prog.* **9**, 523 (1977).
45. Wilson, C. T. R. *J. Franklin Inst.* **208**, 1-12 (1929).
46. Morrison, H. F. *Abnormal Animal Behavior Prior to Earthquakes* (ed. Evernden, J.) 91-94 (US Geological Survey, Menlo Park, 1976).
47. Stuart, W. D. & Johnston, M. J. S. *Geology* **3**, 63-67 (1975).